

# Towards Effective Deep Embedding for Zero-Shot Learning

Lei Zhang<sup>1</sup>, Peng Wang<sup>1</sup>, Lingqiao Liu<sup>1</sup>, Chunhua Shen<sup>1</sup>, Wei Wei<sup>2</sup>, Yannning Zhang<sup>2</sup>, Anton Van Den Hengel<sup>1</sup>

<sup>1</sup>School of Computer Science, The University of Adelaide, Adelaide, 5005, Australia

<sup>2</sup>School of Computer Science, Northwestern Polytechnical University, Xian, 710072, China

{lei.Zhang, peng.wang, lingqiao.liu}@adelaide.edu.au

## Abstract

*Zero-shot learning (ZSL) attempts to recognize visual samples of unseen classes by virtue of the semantic descriptions of those classes. We posit that the key to ZSL is to exploit an effective embedding space where 1) visual samples can be tightly centred around the semantic descriptions of classes that they belong to; 2) visual samples of different classes are separated from each other with a large enough margin. Towards this goal, we present a simple but surprisingly effective deep embedding model. In our model, we separately embed visual samples and semantic descriptions into a latent intermediate space such that visual samples not only coincide with associated semantic descriptions, but also can be correctly discriminated by a trainable linear classifier. By doing this, visual samples can be tightly centred around associated semantic descriptions and more importantly, they can be separated from other semantic descriptions with a large margin, thus leading to a new state-of-the-art for ZSL. Furthermore, due to lacking training samples, the generalization capacity of the learned embedding space to unseen classes can be further improved. To this end, we propose to upgrade our model with a refining strategy which progressively calibrates the embedding space based upon some test samples chosen from unseen classes with high-confidence pseudo labels, and ultimately improves the generalization capacity greatly. Experimental results on five benchmarks demonstrate the great advantage of our model over current state-of-the-art competitors. For example, on AwA1 dataset, our model improves the recognition accuracy on unseen classes by 16.9% in conventional ZSL setting and even by 38.6% in the generalized ZSL setting.*

## 1. Introduction

With the profit from deep learning [15], object recognition [17, 11] has gained great success in recent years. The premise of such success is that sufficient annotated samples for each considered object are available for supervised

learning [15, 17]. However, this is often difficult to comply with in real applications due to the prohibitive annotation cost or some harsh conditions for sample collection (e.g., samples in danger scene, newly emerging or identified) [28, 25]. In many cases [33, 34], there is even no any available annotated samples.

Zero-shot learning (ZSL) [7, 21, 20, 4, 34, 13, 33, 3, 25] has proved to be an effective way to address the above difficulty. In contrast to conventional supervised learning, ZSL attempts to discriminate some *unseen classes* where no annotated samples are available, through exploiting the semantic connections between those classes and some other *seen classes* along with sufficient annotated training samples. This is inspired by the grown human intelligence system which can correctly recognize a new object never seen before according to some basic semantic descriptions of this object. In ZSL, each class name is described by semantic attributes [6], a word vector [23, 7] or a sentence [23], which compose the *semantic space* shared by both seen and unseen classes, while each visual sample (e.g., image) is encoded by a feature vector in the *visual space*.

We posit that the key for ZSL is to exploit an effective embedding space which shows the following two advantages. 1) *Intra-class compactness*. In the embedding space, visual samples from a specific class are tightly centred around the semantic description associated with such a class. 2) *Inter-class separability*. Visual samples from different classes are dispersed with large enough margin. However, most of existing ZSL methods fail to do so and thus suffer from various problems, shown as Table 1. For example, some methods explicitly consider either the semantic space [23, 7, 14, 10] or the visual space [33, 22, 3] as the embedding space. Through learning a nearest neighbourhood (NN) classifier, the embedding space often shows good intra-class compactness. However, the inter-class separability cannot be guaranteed, thus resulting in *hubness problem* [33], especially when visual samples are mapped into a much lower-dimensional semantic space. Although this problem can be mitigated at some extent by exploiting the visual space as the embedding space [33], it is still

Method	Type of embedding space	Intra-class compactness	Inter-class separability	Shortage
DAP, IAP [14], CMT [23], DEVISE [7]	Semantic space	✓	✗	Hubness problem [33]
PSR [3], DEM [33]	Visual space	✓	✗	Hubness problem [33]
CONSE [18], SSE [34], LATEM [30], ALE [1], SJE [2], ESZSL [21], RN [25]	Latent intermediate space	✗	✓	Bias toward seen classes [5]
Ours	Latent intermediate space	✓	✓	None of the above

Table 1. Property of different embedding spaces produced by existing ZSL methods.

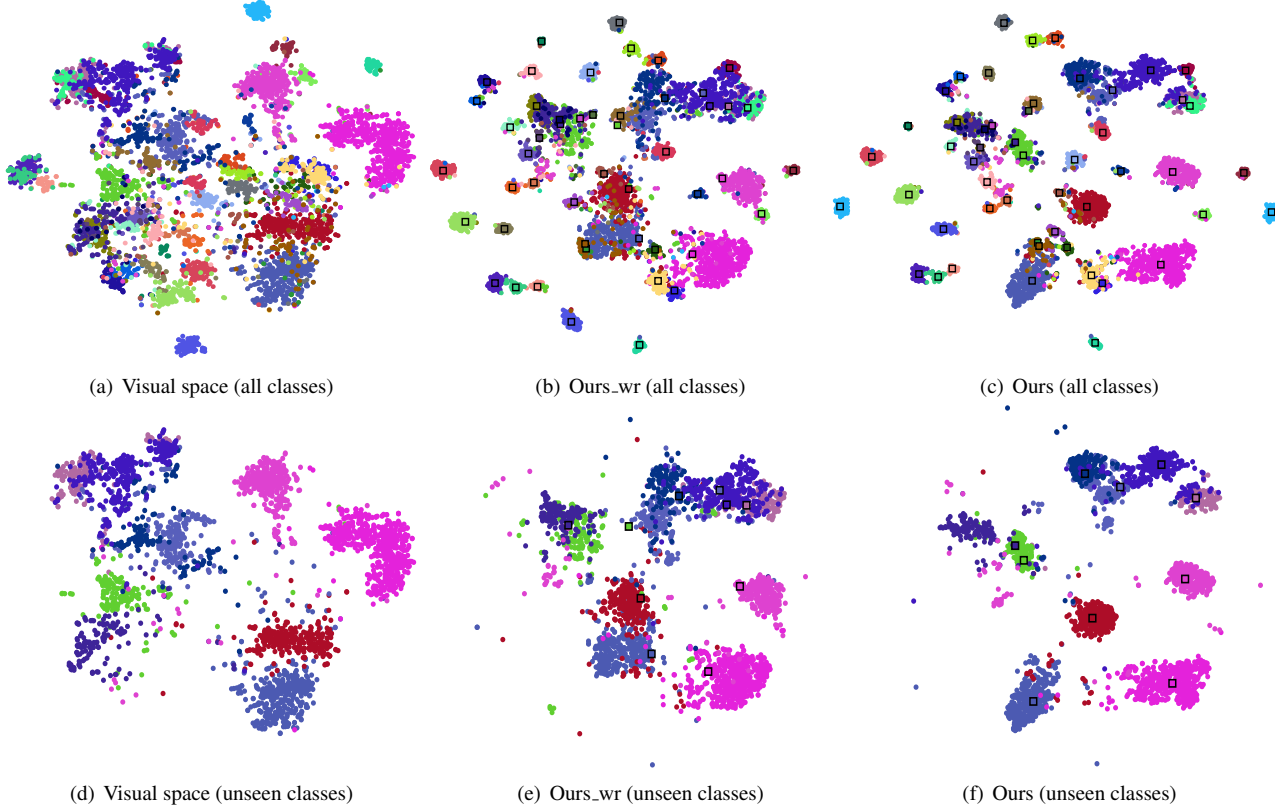


Figure 1. Visualization of the distribution of visual samples from the AwA1 dataset [14] in different embedding spaces, including the visual space [33] and that learned in our model (e.g., 'Ours\_wr' denotes the basic version of our model without refining strategy). In the figure, dots and squares represent the (embedded) visual samples (e.g., encoded with ResNet101 [11] in visual space) and the (embedded) semantic descriptions, respectively. Colors of dots and squares represent various classes. The first row shows the distribution of visual samples from all classes, while the second row shows the distribution of visual samples from unseen classes.

non-negligible, since visual samples even with deep features fail to be dispersed with large enough margin [32], shown as Figure 1(a)(d). In contrast, some other methods [21, 2, 16, 35, 25] project both visual samples and the semantic descriptions into a latent intermediate space via fitting a compatibility function between training samples and semantic descriptions of seen classes for classification. While showing inter-class separability, the resultant embedding space often produces obvious bias towards seen classes [5], i.e., prefers to classify test samples into seen classes.

To exploit an effective embedding space, we present a simple but surprisingly effective deep embedding model. Specifically, we separately embed visual samples and semantic descriptions into a latent intermediate space to ensure that visual samples not only coincide with the associated semantic descriptions, but also can be correctly discriminated by a trainable linear classifier. By doing this, visual samples can be tightly centred around the associated semantic descriptions in the learned embedding space. More importantly, they can be separated from other semantic descriptions with large margin, shown as Figure 1 (b)(e). Both

of these two merits benefit increasing the separability between various classes regardless of having training samples or not, thus leading to a new state-of-the-art for ZSL.

Nevertheless, due to lacking training samples, the generalization capacity of the learned embedding space to unseen classes is still limited. For example, it fails to appropriately center visual samples of unseen classes around the associated semantic descriptions as well as separating any two unseen classes with a large enough margin, shown as Figure 1(e). To address this problem, we propose a refining strategy to upgrade our model. Specifically, in the testing phase, we first choose some high-confidence test samples from unseen classes according to pseudo labels predicted by the current embedding model, and then supplement these samples into training set to calibrate the embedding model through fine-tuning. With repeating this procedure, semantic descriptions of unseen classes can gradually approach the center of the associated visual samples as well as being separated from each other with obvious margin in the learned embedding space, shown as Figure 1(f). Therefore, the generalization capacity to unseen classes is greatly improved. In the experiments on five benchmarks, our model shows great advantage over current state-of-the-arts, e.g., on AwA1 dataset, it improves the recognition accuracy on unseen classes by 16.9% in conventional ZSL setting and even by 38.6% in the generalized ZSL setting.

## 2. Related works

**Embedding model** According to the type of the embedding space, existing ZSL methods can be roughly divided into three groups: 1) *Semantic space*. This group of methods exploit the semantic space as the embedding space [23, 7, 14, 10]. For example, Socher et al. [23] and Frome et al. [7] learn to regress the pre-computed shallow feature or deep features of visual sample into the semantic spaces as well as centring them around the associated semantic descriptions. Then, test samples can be classified by a NN classifier. However, projecting the visual features into a much lower-dimensional semantic space may aggravate the hubness problem [33]. 2) *Visual space*. This line of research learns to embed the semantic descriptions of all classes into the visual space [33, 22]. Recently, Annadani et al. [3] further consider the inter-class semantic relationships (e.g., similar or dissimilar) when learning the embedding space. Profiting from the abundant data diversity in visual space, these methods can mitigate the hubness problem at some extent. Nevertheless, due to the inter-class inseparability problem shown in Figure 1(a)(d), the hubness problem is still non-negligible. 3) *Latent intermediate space*. These methods learn to fit a appropriate compatibility function between visual samples and the semantic descriptions to project both of them into a latent intermediate space [21, 2, 16, 35, 25]. For example, Sung et al. [25] em-

ploy the relation network as the compatibility function and learn it as well as two separate mapping functions in an end-to-end manner. However, due to lacking training samples from unseen classes, the learned comparability function often produces bias results [5]. While our model also exploits a latent embedding space and utilizes a NN classifier, it aims at maximizing both the intra-class compactness and the inter-class separability of latent embedding space. Thus, our model can well mitigate both the hubness and bias problems mentioned above.

**Inductive & transductive ZSL** According to whether the unlabelled test samples from unseen classes are available for training or not, existing ZSL methods can be grouped into two categories. 1) *Inductive ZSL*. For inductive ZSL methods [7, 4, 34, 13, 33, 3, 25], only the labeled samples from seen classes are available in the training phase. 2) *Transductive ZSL*. In contrast, the transductive ZSL methods [8, 12, 9, 24] can access both the labeled samples from seen classes and the unlabelled samples from unseen classes for training, i.e., the partition of test samples (e.g., indicating samples from unseen classes or seen classes) is known in advance. Intuitively, inductive ZSL is more practical and challenging. Although our model also introduces some test samples from unseen classes for model calibration, it is noticeable that the labels as well as the partition of those selected samples are automatically predicted by our model. Such difference enables our model flexible enough to work under both inductive and transductive ZSL settings. In this study, we mainly focus on the inductive ZSL setting.

## 3. Methodology

Provided that a training set with  $N$  samples is given as  $\mathcal{D}_{tr} = \{(\mathbf{x}_i, y_i^s), i = 1, \dots, N\}$ , where  $\mathbf{x}_i$  denotes the  $i$ -th visual sample (e.g., image) with class label  $y_i^s \in \mathcal{Y}^{tr}$  and  $\mathcal{Y}^{tr}$  is the label set of all seen classes. In the testing phase, ZSL aims at predicting the label  $y_j^t \in \mathcal{Y}^{ts}$  for a new sample  $\mathbf{x}_j$ .  $\mathcal{Y}^{ts}$  denotes the label set of all unseen classes and  $\mathcal{Y}^{tr} \cap \mathcal{Y}^{ts} = \emptyset$ . It is noticeable each label  $y_i^s$  or  $y_j^t$  is associated with a semantic description (e.g., attribute vector)  $\mathbf{z}_i^s$  or  $\mathbf{z}_j^t$ . For the generalized ZSL setting [31], the only difference is that the test sample  $\mathbf{x}_j$  may come from the unseen classes or the seen classes, i.e.,  $y_j^t \in \mathcal{Y}^{tr} \cup \mathcal{Y}^{ts}$ .

### 3.1. Proposed deep embedding model

In this study, we attempt to exploit an effective intermediate embedding space which shows both intra-class compactness and the inter-class separability. To this end, we design the architecture of our deep embedding model as Figure 2. In our model, there are two embedding branches which separately embed each visual sample  $\mathbf{x}_i$  and the semantic description  $\mathbf{z}_i^s$  of the class that  $\mathbf{x}_i$  belongs to into a latent intermediate space. In the visual embedding branch, visual sample  $\mathbf{x}_i$  is firstly fed into a deep convolutional sub-

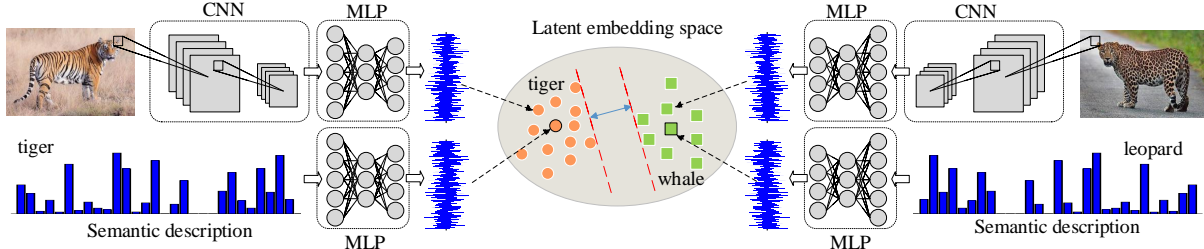


Figure 2. The architecture of the proposed deep embedding model.

net for initial encoding. Then, the encoded  $\mathbf{x}_i$  is mapped into the latent embedding space by a multilayer perceptron unit. In the semantic embedding branch, the semantic description  $\mathbf{z}_i^s$  is directly embedded into the latent embedding space by a multilayer perceptron unit.

Two-branch embedding structure has been employed in some previous works [16, 2]. Different from these works [16, 2] that exploits a latent embedding space implicitly via learning a compatibility function between visual samples and the associated semantic descriptions for classification [16, 2], we propose to explicitly optimize the latent embedding space by maximizing both the intra-class compactness and the inter-class separability within a well-designed optimization problem. On one hand, since the key for intra-class compactness is to eliminate the visual-semantic gap, we propose to minimize the distance (e.g., Euclidean distance) between the visual sample  $\mathbf{x}_i$  and the corresponding semantic description  $\mathbf{z}_i^s$  in the latent embedding space [23, 33]. On the other hand, considering that the well-separated samples from various classes in general can be appropriately discriminated by a linear classifier [26, 11], we propose to minimize the misclassification loss of visual samples in the latent embedding space with a trainable linear classifier to maximize the inter-class separability. Inspired by these two points, the proposed deep embedding model can be formulated as

$$\begin{aligned} \min_{\theta_v, \theta_s, \mathbf{W}} \sum_{i=1}^N & \|\phi_{\theta_v}(\mathbf{x}_i) - \psi_{\theta_s}(\mathbf{z}_i^s)\|_2^2 + \lambda \mathcal{L}(\mathbf{W}^T \phi_{\theta_v}(\mathbf{x}_i), y_i^s) \\ & + \eta (\|\theta_v\|_2^2 + \|\theta_s\|_2^2 + \|\mathbf{W}\|_2^2), \end{aligned} \quad (1)$$

where  $\phi_{\theta_v}(\cdot)$  and  $\psi_{\theta_s}(\cdot)$  denote the MLP units in the visual and semantic embedding branches, respectively.  $\theta_v$  and  $\theta_s$  are the parameters included in these two MLP units. It is noticeable that we still utilize  $\mathbf{x}_i$  to represent the encoded result (e.g., pre-trained deep feature [31]) of the visual sample to avoid the abuse of notations.  $\mathbf{W}$  is the weight matrix in the linear classifier and  $\mathcal{L}(\cdot)$  measures the loss of misclassification. To avoid over-fitting, we further regularize the  $\ell_2$  norm of all parameters.  $\lambda$  and  $\eta$  are two balance scalars.

Given the learned parameter  $\theta_v$  and  $\theta_s$ , the label for a

test sample  $\mathbf{x}_j^t$  can be predicted as

$$\hat{y}_j^t = \min_{y \in \mathcal{Y}^{ts}} \|\phi_{\theta_v}(\mathbf{x}_j^t) - \psi_{\theta_s}(\mathbf{z})\|_2^2 \quad (2)$$

where  $\mathbf{z}$  denotes the semantic description associated with the label  $y$ . For the generalized ZSL setting, we only need to modify the solution space of label as  $y \in \mathcal{Y}^{tr} \cup \mathcal{Y}^{ts}$ .

**Hubness problem** In contrast to [33] that attempts to avoid aggravating the hugeness problems by virtue of sample variety in visual space, our model in Eq. (1) is able to explicitly address the hubness problem through regularizing the inter-class separability of the embedding space. For example, if a given visual sample  $\mathbf{x}_i$  stays close to the semantic descriptions of several different classes, it is likely to be misclassified by a simple linear classifier and ultimately increases the value of the objective function in Eq. (1). Therefore, the hubness problem can be well mitigated via minimizing the objective function in Eq. (1). A visualization example of the latent embedding space learned by our model is shown in Figure 1(b)(e). Compared with the embedding space in [33] as Figure 1(a)(d), visual samples are more tightly centred around their corresponding semantic descriptions. Moreover, the separability between any two different classes regardless of seen or unseen is enlarged. The hubness problem thus is mitigated obviously.

**Bias problem** It has been shown that fitting a compatibility function for the inter-class separability is prone to produce bias towards seen classes [5]. In our model, we consider both the intra-class compactness and the inter-class separability and learn to fit a NN classifier as Eq. (2), which enables the embedding space to accurately discriminate the unseen classes from those seen ones, thus well mitigating the bias problem. For example, in Figure 1, our model obviously enlarges the separability between seen classes and unseen ones. More evidence can be found in Table 2 and 3.

### 3.2. Refining strategy

Although the learned embedding space has shown promising intra-class compactness and inter-class separability as Figure 1(b), due to lacking training samples, the generalization capacity to unseen classes is still limited. An example can be seen in Figure 1(e), where visual samples fail

to be centred around the corresponding semantic descriptions as well as being separated from other unseen classes with obvious margin. To address this problem, we propose a refining strategy to upgrade the proposed model in Eq. (1) to a more general version.

Specifically, given a set of test samples, we first predict their pseudo labels with the model in Eq. (2) given semantic descriptions. Then, according to the visual-semantic gap (e.g.,  $\|\phi_{\theta_v}(\mathbf{x}_j^t) - \psi_{\theta_s}(\mathbf{z})\|_2^2$ ) and pseudo labels, we select the top- $M$  high-confidence test samples for each unseen class and supplement those samples into the training set  $\mathcal{D}_{tr}$  as data augmentation. With the augmented  $\mathcal{D}_{tr}$ , we calibrate the learned embedding space as

$$\begin{aligned} \min_{\theta_v, \theta_s, \mathbf{W}} & \sum_{i=1}^N \|\phi_{\theta_v}(\mathbf{x}_i) - \psi_{\theta_s}(\mathbf{z}_i^s)\|_2^2 + \lambda \mathcal{L}(\mathbf{W}^T \phi_{\theta_v}(\mathbf{x}_i), y_i^s) \\ & + \sum_{i=1}^{CM} \|\phi_{\theta_v}(\tilde{\mathbf{x}}_i) - \psi_{\theta_s}(\tilde{\mathbf{z}}_i^s)\|_2^2 + \lambda \mathcal{L}(\mathbf{W}^T \phi_{\theta_v}(\tilde{\mathbf{x}}_i), \tilde{y}_i^s) \\ & + \eta (\|\theta_v\|_2^2 + \|\theta_s\|_2^2 + \|\mathbf{W}\|_2^2), \end{aligned} \quad (3)$$

where  $C$  denotes the number of unseen classes and  $\tilde{\mathbf{x}}_i$  is the  $i$ -th selected sample.  $\tilde{y}_i^s$  and  $\tilde{\mathbf{z}}_i^s$  are the corresponding pseudo label and the semantic description.

With optimizing Eq. (3), the visual-semantic loss, e.g.,  $\|\phi_{\theta_v}(\tilde{\mathbf{x}}_i) - \psi_{\theta_s}(\tilde{\mathbf{z}}_i^s)\|_2^2$ , encourages the semantic description  $\tilde{\mathbf{z}}_i^s$  of a specific class to approach the center of visual samples  $\tilde{\mathbf{x}}_i$  belonging to this class. Moreover, the classification loss, e.g.,  $\mathcal{L}(\mathbf{W}^T \phi_{\theta_v}(\tilde{\mathbf{x}}_i), \tilde{y}_i^s)$ , benefits increasing the separability between any two unseen classes. Therefore, the refining strategy above is able to improve the generalization capacity to unseen classes, i.e., prediction accuracy. Inspired by this point, we can repeat the procedure to progressively calibrate the embedding space with increasing selected samples. To avoid misleading the calibration with incorrectly labelled samples, we set  $M$  with a small enough value at beginning to ensure selecting correctly labelled samples and then gradually increase  $M$  to select more samples with the increase of generalization capacity.

Figure 1 (c)(f) shows an example of the embedding space learned by Eq. (3) after 9 rounds of calibration. It can be seen that in the resultant embedding space, visual samples of unseen classes are tightly centred around the associated semantic descriptions and different unseen classes are also separated from each other with obvious margin.

It is noticeable that the refining strategy upgrades our model to a on-line version. When a batch of new test images are available, we can calibrate the learned embedding space accordingly to improve the generalization capacity to unseen classes. Thus, our model is effective in practice and can be applied to both conventional ZSL and the generalized ZSL, which can be further demonstrated in Section 5.

## 4. Optimization

Since Eq. (1) and Eq. (3) show the same structure, we take Eq. (1) as an example to show how to optimize our model in the training phase. Considering that  $\theta_v$  is coupled with  $\theta_s$  in the objective function, we adopt the alternative minimizing scheme [32] to reduce the original optimization problem in Eq. (1) into two subproblems and then alternatively optimize each subproblem until convergence. In this study, we term these two subproblems, the visual embedding problem and the semantic embedding problem, respectively, which can be formulated as follows.

**Visual embedding problem.** Given  $\theta_s^{(t)}$  in the  $t$ -th iteration, we can estimate  $\theta_s^{(t+1)}$  and  $\mathbf{W}^{(t+1)}$  by solving the following problem

$$\begin{aligned} \min_{\theta_v, \mathbf{W}} & \sum_{i=1}^N \|\phi_{\theta_v}(\mathbf{x}_i) - \psi_{\theta_s^{(t)}}(\mathbf{z}_i^s)\|_2^2 + \lambda \mathcal{L}(\mathbf{W}^T \phi_{\theta_v}(\mathbf{x}_i), y_i^s) \\ & + \eta (\|\theta_v\|_2^2 + \|\mathbf{W}\|_2^2). \end{aligned} \quad (4)$$

**Semantic embedding problem.** Given the estimated  $\theta_v^{(t+1)}$ , the subproblem for estimating  $\theta_s^{(t+1)}$  can be formulated as

$$\min_{\theta_s} \sum_{i=1}^N \|\phi_{\theta_v^{(t+1)}}(\mathbf{x}_i) - \psi_{\theta_s}(\mathbf{z}_i^s)\|_2^2 + \eta \|\theta_s\|_2^2, \quad (5)$$

Since both the objective functions above are differential, we adopt back-propagation algorithm [11] to solve each subproblem. The overall flow for training our model is summarized into Algorithm 1. It can be seen that our model degenerates to the basic version in Eq. (1) without refining strategy when  $R = 1$ .

## 5. Experiment

### 5.1. Datasets and settings

**Datasets** Following the GUB settings in [31], we select five benchmarks for evaluation: **AwA1** [14] contains 30,745 images of 50 classes of animals where 40 classes are seen while the remaining 10 classes are unseen during training. Each class is associated with a 85-dimension continuous attribute vector. **AwA2** [31] is an extension of **AwA1** and consists of 37,322 images of the same 50 classes of animals. **CUB** (Caltech-UCSD Birds-200-2011) [29] contains 11,788 images of 200 bird species. We split these bird species into 150 seen classes with 50 disjoint unseen classes and annotate each of them with a 312-dimension continuous attribute vector for evaluation. **SUN** [19] consists of 14340 images of scenes coming from 717 categories where 645 classes are selected for training and the remaining 72 classes are used for testing. A 102-dimension continuous attribute vector is utilized to describe the semantic information of each class. **aPY** (Attribute Pascal and

---

**Algorithm 1:** Training the proposed model

---

**Input:** Training dataset  $\mathcal{D}_{tr}$ , test images  $\{\mathbf{x}_j^t\}$ , semantic descriptions for all classes, scalar  $\lambda$  and  $\eta$ ;

**Outer loop:** for  $r = 1, 2, \dots, R$  **do**

1. Learning latent embedding space:  
**Inner loop:** for  $t = 1, 2, \dots, T$  **do**
  - (a) Solve visual embedding problem as Eq. (4);
  - (b) Solve semantic embedding problem as Eq. (5);**End for**
2. Training dataset augmentation;
  - (a) Predict  $\{\hat{y}_j^t\}$  for  $\{\mathbf{x}_j^t\}$  as Eq. (2);
  - (b) Select the top- $M$  high-confidence samples from each unseen class;
  - (c) Augment  $\mathcal{D}_{tr}$  with selected samples;
  - (d) Update  $M = M * (r + 1)$ ;

**End for**

**Output:** Model parameters  $\theta_v, \theta_s, \mathbf{W}$  and labels  $\{\hat{y}_j^t\}$ .

---

Yahoo) [6] contains 32 classes with 64-dimension attribute vectors. Among them, we utilize 20 Pascal classes for training and 12 Yahoo classes for testing.

**ZSL settings** In this study, we conduct experiments under two kinds of ZSL settings, including the conventional ZSL setting [24] and the generalized ZSL setting [25]. In the convention ZSL, test samples are restricted to the unseen classes, while in the generalized ZSL, they may come from either seen classes or unseen classes.

**Implementation details** Following the GUB settings in [31], we adopt the 2048-dimension top pooling units of ResNet101 [11] as the initial encoding in the visual embedding branch. In addition, we utilize a fully connected (FC) linear + Rectified Linear Unit (ReLU) layer as the MLP unit for visual embedding, while two FC+ReLU layers as the MLP unit for semantic embedding. The dimension of the latent embedding space is fixed at 1024. In the MLP for semantic embedding, the dimension of the output of the first FC+ReLU layer is set as the mean of the dimensions of the input semantic description and the latent embedding space. During training, we adopt the cross entropy loss as  $\mathcal{L}(\cdot)$ . The scalar  $\lambda$  and  $\eta$  are determined by cross validation on each benchmark. We implement our model with Pytorch platform and train it with Adam optimizer with learning rate  $1e^{-4}$ . In Algorithm 1, the maximal iteration of the outer loop is set as  $R = 10$ . The inner loop is implemented by the back propagation algorithm where the maximal epoch is set as 50. The initial number of selected samples is set as  $M = 40$ . For simplicity, our model and its basic version without refining strategy is denoted as 'Ours' and 'Ours\_wr', respectively, in the following experiments.

**Competitors** To demonstrate the effectiveness of our

Method	<b>AwA1</b>	<b>AwA2</b>	<b>CUB</b>	<b>SUN</b>	<b>aPY</b>
DAP [14]	44.1	46.1	40.0	39.9	33.8
IAP [14]	35.9	35.9	24.0	19.4	36.6
CONSE [18]	45.6	44.5	34.3	38.8	26.9
CMT [23]	39.5	37.9	34.6	39.9	28.0
SSE [34]	60.1	61.0	43.9	51.5	34.0
LATEM [30]	55.1	55.8	49.3	55.3	35.2
ALE [1]	59.9	62.5	54.9	58.1	39.7
DEVISE [7]	54.2	59.7	52.0	56.5	<b>39.8</b>
SJE [2]	65.6	61.9	53.9	53.7	32.9
ESZSL [21]	58.2	58.6	53.9	54.5	<b>38.3</b>
SYNC [4]	54.0	46.6	55.6	56.3	23.9
SAE [13]	53.0	54.1	33.3	40.3	8.3
GFZSL [27]	68.3	63.8	49.3	60.6	38.4
PSR [3]	-	63.8	56.0	61.4	38.4
DEM [33]	68.4	<b>67.1</b>	51.7	40.3	35.0
RN [25]	68.2	64.2	55.6	-	-
Ours_wr	<b>70.1</b>	66.5	<b>57.1</b>	<b>62.4</b>	20.4
Ours	<b>85.3</b>	<b>77.5</b>	<b>67.8</b>	<b>61.6</b>	31.3

Table 2. Recognition accuracy of all methods on five benchmarks under the conventional ZSL setting.

model, we compare it with 16 existing ZSL methods. Among them, 13 methods are the baselines adopted in [31], namely DAP [14], IAP [14], CONSE [18], CMT [23], SSE [34], LATEM [30], ALE [1], DEVISE [7], SJE [2], ESZSL [21], SYNC [4], SAE [13] and GFZSL [27]. In addition, we further select another three recent state-of-the-art ZSL methods, including PSR [3], DEM [33] and RN [25].

## 5.2. Comparison in conventional ZSL

In the conventional ZSL, we follow the experiment and evaluation setting as [31]. The average recognition accuracy of all methods on unseen classes from five benchmarks are reported in Table 2. The results of 13 baselines are from [31], while the results of these three state-of-the-art methods (e.g., PSR [3], DEM [33] and RN [25]) are from the reference papers and Github pages of authors. Since the results of all methods are obtained under the GUB settings [31], the comparison in Table 2 is fair. It can be seen that Ours\_wr obviously outperforms DAP, DIP, CMT and DEVISE, which exploit the semantic space as the embedding space. For example, Ours\_wr outperforms DEVISE by 15.9% on AwA1 dataset. This is because these methods suffer a lot from the hubness problem, while our model can well mitigate this problem by explicitly regularizing the inter-class separability. Although DEM and PSR also can mitigate the hubness problem at some extent, they still suffer more from this problem than our model. For example, Ours\_wr surpasses PSR by 2.7% on AwA2 dataset, and even outperforms DEM by 22.1% on the SUN dataset.

Method	AwA1			AwA2			CUB			SUN			aPY		
	ts	tr	H												
DAP [14]	0.0	88.7	0.0	0.0	84.7	0.0	1.7	<b>67.9</b>	3.3	4.2	25.1	7.2	4.8	78.3	9.0
IAP [14]	2.1	78.2	4.1	0.9	87.6	1.8	0.2	<b>72.8</b>	0.4	1.0	37.8	1.8	5.7	65.6	10.4
CONSE [18]	0.4	88.6	0.8	0.5	90.6	1.0	1.6	<b>72.2</b>	3.1	6.8	<b>39.9</b>	11.6	0.0	<b>91.2</b>	0.0
CMT [23]	0.9	87.6	1.8	0.5	90.0	1.0	7.2	49.8	12.6	8.1	21.8	11.8	1.4	<b>85.2</b>	2.8
CMT* [23]	8.4	86.9	15.3	8.7	89.0	15.9	4.7	60.1	8.7	8.7	28.0	13.3	10.9	74.2	19.0
SSE [34]	7.0	80.5	12.9	8.1	82.5	14.8	8.5	46.9	14.4	2.1	36.4	4.0	0.2	78.9	0.4
LATEM [30]	7.3	71.7	13.3	11.5	77.3	20.0	15.2	57.3	24.0	14.7	28.8	19.5	0.1	73.0	0.2
ALE [1]	16.8	76.1	27.5	14.0	81.8	23.9	<b>23.7</b>	62.8	34.4	21.8	33.1	26.3	4.6	73.7	8.7
DEVISE [7]	13.4	68.7	22.4	17.1	74.7	27.8	23.8	53.0	32.8	16.9	27.4	20.9	4.9	76.9	9.2
SJE [2]	11.3	74.6	19.6	8.0	73.9	14.4	23.5	<b>59.2</b>	33.6	14.7	30.5	19.8	3.7	55.7	6.9
ESZSL [21]	6.6	75.6	12.1	5.9	77.8	11.0	12.6	63.8	21.0	11.0	27.9	15.8	2.4	70.1	4.6
SYNC [4]	8.9	87.3	16.2	10.0	90.5	18.0	11.5	70.9	19.8	7.9	<b>43.3</b>	13.4	7.4	66.3	13.3
SAE [13]	1.8	77.1	3.5	1.1	82.2	2.2	7.8	54.0	13.6	8.8	18.0	11.8	0.4	80.9	0.9
GFZSL [27]	1.8	80.3	3.5	2.5	80.1	4.8	0.0	45.7	0.0	0.0	39.6	0.0	0.0	83.3	0.0
PSR [3]	-	-	-	20.7	73.8	32.3	24.6	54.3	33.9	20.8	37.2	26.7	13.5	51.4	21.4
DEM [33]	32.8	84.7	47.3	30.5	86.4	45.1	19.6	<b>57.9</b>	29.2	20.5	34.3	25.6	<b>11.1</b>	75.1	<b>19.4</b>
RN [25]	31.4	<b>91.3</b>	46.7	30.0	<b>93.4</b>	45.3	38.1	61.4	<b>47.0</b>	-	-	-	-	-	-
Ours_wr	<b>36.9</b>	<b>90.6</b>	<b>52.4</b>	<b>35.2</b>	93.0	<b>51.1</b>	21.0	66.0	31.9	<b>22.1</b>	35.6	<b>27.3</b>	7.8	75.3	14.1
Ours	<b>71.4</b>	90.1	<b>79.7</b>	<b>68.4</b>	<b>93.2</b>	<b>78.9</b>	<b>54.0</b>	62.9	<b>58.1</b>	<b>47.2</b>	38.5	<b>42.4</b>	<b>29.8</b>	79.4	<b>43.3</b>

Table 3. Recognition accuracy of all methods on five benchmarks under the generalized ZSL setting. **ts** denotes the average recognition accuracy on unseen classes, while **tr** denotes the average recognition accuracy on seen classes. **H** denotes the harmonic mean. (CMT\*: CMT with novelty detection)

Similar as this study, the rest of competitors mainly focus on exploiting a latent intermediate embedding space. Among them, RN achieves the state-of-the-art performance. Nevertheless, since considering both the intra-class compactness and the inter-class separability enables our model being immune to the bias problem, `Ours_wr` still slightly outperforms RN, e.g., by 2.3% on the AwA2 dataset. These results above demonstrate that both the intra-class compactness and the inter-class separability are crucial to exploit an effective embedding space for ZSL.

In addition, we find that `Ours` with refining strategy outperforms the state-of-the-art competitors in most cases with a much larger margin than `Ours_wr`. In particular, on the CUB dataset, `Ours` outperforms the most competitive method, i.e., PSR, by 11.8%, while on the AwA1 dataset, the improvement over the most competitive method, i.e., DEM, is even up to 16.9%. This is because given a batch of test samples, `Ours` can progressively calibrate the embedding space based on some test samples selected from unseen classes. This enables `Ours` to generalize better to unseen classes than other competitors which never access samples of unseen classes. On the aPY dataset, `Ours` is less than the state-of-the-art methods. However, `Ours` performs much better under the generalized ZSL setting, which will be introduced in the following.

### 5.3. Comparison in generalized ZSL

Due to considering both the intra-class compactness and the inter-class separability of the embedding space, our model is more appropriate to cope with the generalized ZSL problem. To clarify this point, we follow the generalized ZSL setting in [31] and report the recognition accuracy of all methods in Table 3. The results of all competitors are obtained in the same way as Section 5.2. We can find that `Ours_wr` outperforms all competitors in many cases, especially in the recognition accuracy on unseen classes. For example, compared with the most competitive DEM, `Ours_wr` improves the recognition accuracy on unseen classes by 4.7% on AwA2 dataset. This demonstrates that our model is effective in discriminating each unseen class from other unseen classes as well as seen classes.

With the refining strategy, the performance of our model is still greatly improved. For example, compared with other competitors on CUB dataset, `Ours` improves the recognition accuracy on unseen classes by 15.9% at least, and the improvement is even up to 39.6% on the AwA1 dataset. This proves that the proposed refining strategy is able to obviously improve the generalization capacity of our model to unseen classes. In addition, most of competitors in Table 3 produce obvious bias towards seen classes, i.e., the recognition accuracy on unseen class are much less than that on

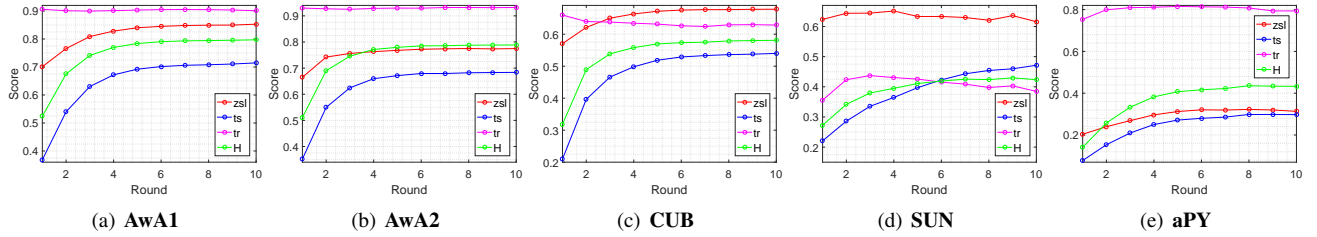


Figure 3. Curves of recognition accuracy of Ours versus round of model calibration on five benchmarks. 'zsl' denotes the accuracy under conventional ZSL setting. 'ts', 'tr' and 'H' denotes measures (e.g., accuracy on unseen classes, accuracy on seen classes and the harmonic mean) under generalized ZSL setting.

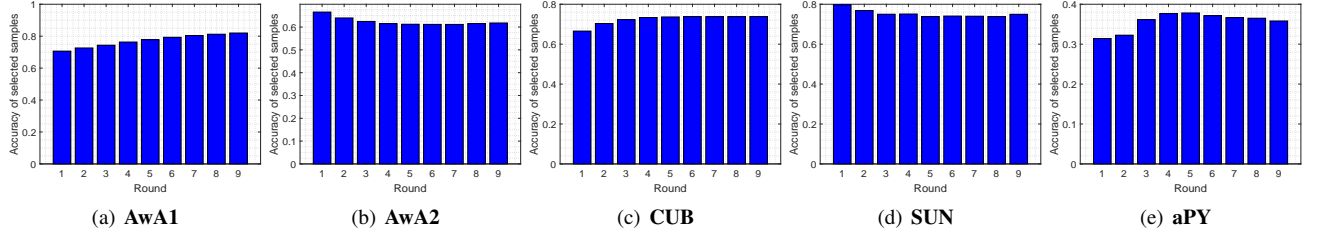


Figure 4. Prediction accuracy of selected test samples of unseen classes within 9 rounds of model calibration under generalized ZSL setting.

seen classes, while Ours produces much more balanced results. This makes Ours gain the best harmonic mean scores on all five benchmarks with big margin from other competitors. For example, on AwA2 dataset, the harmonic mean of Ours is larger than that of all competitors by 33.6% at least. These results demonstrate the superiority of our model in addressing the bias problem.

#### 5.4. Further discussion

In this section, we conduct experiments to justify the effectiveness of the refining strategy and regularizing inter-class separability.

**Effectiveness of refining strategy** To clarify this point, we plot the recognition accuracy curves of Ours on five benchmarks versus the round (i.e.,  $R$ ) of model calibration in Figure 3. It can be seen that with the increase of round, the recognition accuracy on unseen classes is gradually improved and ultimately converges. The reason is intuitive. At the beginning, to avoid introducing too much incorrectly labelled samples and mislead the learning of embedding space, we only select very limited samples from unseen classes that fail to comprehensively depict the distribution of each unseen class. The learned embedding space thus can be further improved. With the increase of round, i.e., more and more correctly labelled samples are introduced, the generalization capacity of the embedding space is gradually increased and ultimately converges when no extra information is introduced. In contrast, the recognition accuracy on seen classes stays stable, shown as the curve of 'tr' in Figure 3. This is because we do not introduce any new samples from seen class. We also have tried to se-

lect new samples from seen classes during testing. However, no obvious improvement on the recognition accuracy of seen classes is observed, since extensive training samples from seen classes have conveyed sufficient information for classification, e.g., on AwA2, the recognition accuracy of Ours\\_wr on seen classes is up to 93.0%.

The premise of the success of the refining strategy is that most of the selected samples are labelled correctly. To clarify this point, we show the prediction accuracy of selected samples in each round of the dynamic refining strategy in Figure 4. We find that the prediction accuracy of first round is over 70% in most benchmarks. With the increase of round, the prediction accuracy stays almost stable. Since we gradually increase  $M$  in each round, more and more correctly labelled samples will be selected for model calibration. On the aPY dataset, although the prediction accuracy is only around 30%, selected samples still can provide useful information to improve the generalization capacity to unseen classes, since the recognition accuracy of unseen classes obtained by Ours\\_wr is less than 10%.

**Effectiveness of regularizing intra-class separability** To clarify this, we conduct experiments on AwA1 dataset with Ours\\_wr and Ours given different  $\lambda$ . The results are summarized into Figure 5. It can be seen that our model performs stably with a wide range of  $\lambda$ , especially Ours\\_wr. When  $\lambda = 0$ , the resultant embedding model collapses. This is owing to that we separately map the visual samples and the semantic descriptions into a latent embedding space. When  $\lambda = 0$ , trivial solutions will be reached, e.g., visual samples and semantic descriptions from different classes are mapped into the same point. Therefore, regularizing the

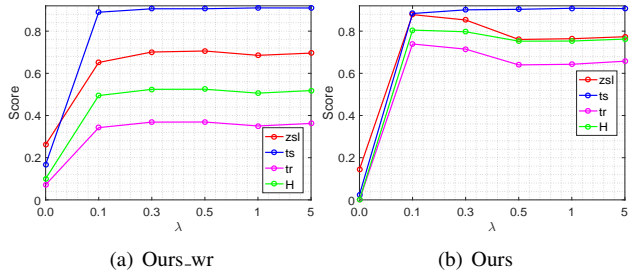


Figure 5. Recognition accuracy of the proposed model with different  $\lambda$ . 'zsl' denotes the accuracy under conventional ZSL setting. 'ts', 'tr' and 'H' denotes measures (e.g., accuracy on unseen classes, accuracy on seen classes and the harmonic mean) under generalized ZSL setting.

inter-class separability is crucial for our model.

In addition, regularizing the intra-class compactness is also crucial for our model. The reason is intuitive. When removing the intra-class compactness (e.g.,  $\|\phi_{\theta_v}(\mathbf{x}_i) - \phi_{\theta_s}(\mathbf{z}_i^s)\|_2^2$ ) in Eq. (1), our model is disabled for ZSL.

## References

- [1] Z. Akata, F. Perronnin, Z. Harchaoui, and C. Schmid. Label-embedding for image classification. *IEEE transactions on pattern analysis and machine intelligence*, 38(7):1425–1438, 2016. [2](#), [6](#), [7](#)
- [2] Z. Akata, S. Reed, D. Walter, H. Lee, and B. Schiele. Evaluation of output embeddings for fine-grained image classification. In *Proceedings of the IEEE Conference on Computer Vision and Pattern Recognition*, pages 2927–2936, 2015. [2](#), [3](#), [4](#), [6](#), [7](#)
- [3] Y. Annadani and S. Biswas. Preserving semantic relations for zero-shot learning. In *Proceedings of the IEEE Conference on Computer Vision and Pattern Recognition*, pages 7603–7612, 2018. [1](#), [2](#), [3](#), [6](#), [7](#)
- [4] S. Changpinyo, W.-L. Chao, B. Gong, and F. Sha. Synthesized classifiers for zero-shot learning. In *Proceedings of the IEEE Conference on Computer Vision and Pattern Recognition*, pages 5327–5336, 2016. [1](#), [3](#), [6](#), [7](#)
- [5] W.-L. Chao, S. Changpinyo, B. Gong, and F. Sha. An empirical study and analysis of generalized zero-shot learning for object recognition in the wild. In *European Conference on Computer Vision*, pages 52–68. Springer, 2016. [2](#), [3](#), [4](#)
- [6] A. Farhadi, I. Endres, D. Hoiem, and D. Forsyth. Describing objects by their attributes. In *Computer Vision and Pattern Recognition, 2009. CVPR 2009. IEEE Conference on*, pages 1778–1785. IEEE, 2009. [1](#), [6](#)
- [7] A. Frome, G. S. Corrado, J. Shlens, S. Bengio, J. Dean, T. Mikolov, et al. Devise: A deep visual-semantic embedding model. In *Advances in neural information processing systems*, pages 2121–2129, 2013. [1](#), [2](#), [3](#), [6](#), [7](#)
- [8] Y. Fu, T. M. Hospedales, T. Xiang, Z. Fu, and S. Gong. Transductive multi-view embedding for zero-shot recognition and annotation. In *European Conference on Computer Vision*, pages 584–599. Springer, 2014. [3](#)
- [9] Y. Fu, T. M. Hospedales, T. Xiang, and S. Gong. Transductive multi-view zero-shot learning. *IEEE transactions on pattern analysis and machine intelligence*, 37(11):2332–2345, 2015. [3](#)
- [10] Y. Fu and L. Sigal. Semi-supervised vocabulary-informed learning. In *Proceedings of the IEEE Conference on Computer Vision and Pattern Recognition*, pages 5337–5346, 2016. [1](#), [3](#)
- [11] K. He, X. Zhang, S. Ren, and J. Sun. Deep residual learning for image recognition. In *Proceedings of the IEEE conference on computer vision and pattern recognition*, pages 770–778, 2016. [1](#), [2](#), [4](#), [5](#), [6](#)
- [12] E. Kodirov, T. Xiang, Z. Fu, and S. Gong. Unsupervised domain adaptation for zero-shot learning. In *Proceedings of the IEEE International Conference on Computer Vision*, pages 2452–2460, 2015. [3](#)
- [13] E. Kodirov, T. Xiang, and S. Gong. Semantic autoencoder for zero-shot learning. In *2017 IEEE Conference on Computer Vision and Pattern Recognition (CVPR)*, pages 4447–4456. IEEE, 2017. [1](#), [3](#), [6](#), [7](#)
- [14] C. H. Lampert, H. Nickisch, and S. Harmeling. Attribute-based classification for zero-shot visual object categorization. *IEEE Transactions on Pattern Analysis and Machine Intelligence*, 36(3):453–465, 2014. [1](#), [2](#), [3](#), [5](#), [6](#), [7](#)
- [15] Y. LeCun, Y. Bengio, and G. Hinton. Deep learning. *nature*, 521(7553):436, 2015. [1](#)
- [16] J. Lei Ba, K. Swersky, S. Fidler, et al. Predicting deep zero-shot convolutional neural networks using textual descriptions. In *Proceedings of the IEEE International Conference on Computer Vision*, pages 4247–4255, 2015. [2](#), [3](#), [4](#)
- [17] M. Liang and X. Hu. Recurrent convolutional neural network for object recognition. In *Proceedings of the IEEE Conference on Computer Vision and Pattern Recognition*, pages 3367–3375, 2015. [1](#)
- [18] M. Norouzi, T. Mikolov, S. Bengio, Y. Singer, J. Shlens, A. Frome, G. S. Corrado, and J. Dean. Zero-shot learning by convex combination of semantic embeddings. *arXiv preprint arXiv:1312.5650*, 2013. [2](#), [6](#), [7](#)
- [19] G. Patterson and J. Hays. Sun attribute database: Discovering, annotating, and recognizing scene attributes. In *Computer Vision and Pattern Recognition (CVPR), 2012 IEEE Conference on*, pages 2751–2758. IEEE, 2012. [5](#)
- [20] R. Qiao, L. Liu, C. Shen, and A. van den Hengel. Less is more: zero-shot learning from online textual documents with noise suppression. In *Proceedings of the IEEE Conference on Computer Vision and Pattern Recognition*, pages 2249–2257, 2016. [1](#)
- [21] B. Romera-Paredes and P. Torr. An embarrassingly simple approach to zero-shot learning. In *International Conference on Machine Learning*, pages 2152–2161, 2015. [1](#), [2](#), [3](#), [6](#), [7](#)
- [22] Y. Shigeto, I. Suzuki, K. Hara, M. Shimbo, and Y. Matsumoto. Ridge regression, hubness, and zero-shot learning. In *Joint European Conference on Machine Learning and Knowledge Discovery in Databases*, pages 135–151. Springer, 2015. [1](#), [3](#)
- [23] R. Socher, M. Ganjoo, C. D. Manning, and A. Ng. Zero-shot learning through cross-modal transfer. In *Advances in neural*

*information processing systems*, pages 935–943, 2013. 1, 2, 3, 4, 6, 7

[24] J. Song, C. Shen, Y. Yang, Y. Liu, and M. Song. Transductive unbiased embedding for zero-shot learning. In *Proceedings of the IEEE Conference on Computer Vision and Pattern Recognition*, pages 1024–1033, 2018. 3, 6

[25] F. Sung, Y. Yang, L. Zhang, T. Xiang, P. H. Torr, and T. M. Hospedales. Learning to compare: Relation network for few-shot learning. In *The IEEE Conference on Computer Vision and Pattern Recognition (CVPR)*, June 2018. 1, 2, 3, 6, 7

[26] P. Upchurch, J. R. Gardner, G. Pleiss, R. Pless, N. Snavely, K. Bala, and K. Q. Weinberger. Deep feature interpolation for image content changes. In *CVPR*, pages 6090–6099, 2017. 4

[27] V. K. Verma and P. Rai. A simple exponential family framework for zero-shot learning. In *Joint European Conference on Machine Learning and Knowledge Discovery in Databases*, pages 792–808. Springer, 2017. 6, 7

[28] O. Vinyals, C. Blundell, T. Lillicrap, D. Wierstra, et al. Matching networks for one shot learning. In *Advances in Neural Information Processing Systems*, pages 3630–3638, 2016. 1

[29] C. Wah, S. Branson, P. Perona, and S. Belongie. Multiclass recognition and part localization with humans in the loop. In *Computer Vision (ICCV), 2011 IEEE International Conference on*, pages 2524–2531. IEEE, 2011. 5

[30] Y. Xian, Z. Akata, G. Sharma, Q. Nguyen, M. Hein, and B. Schiele. Latent embeddings for zero-shot classification. In *Proceedings of the IEEE Conference on Computer Vision and Pattern Recognition*, pages 69–77, 2016. 2, 6, 7

[31] Y. Xian, C. H. Lampert, B. Schiele, and Z. Akata. Zero-shot learning—a comprehensive evaluation of the good, the bad and the ugly. *arXiv preprint arXiv:1707.00600*, 2017. 3, 4, 5, 6, 7

[32] L. Zhang, P. Wang, W. Wei, H. Lu, C. Shen, A. van den Hengel, and Y. Zhang. Unsupervised domain adaptation using robust class-wise matching. *IEEE Transactions on Circuits and Systems for Video Technology*, 2018. 2, 5

[33] L. Zhang, T. Xiang, and S. Gong. Learning a deep embedding model for zero-shot learning. In *Proceedings of the IEEE Conference on Computer Vision and Pattern Recognition*, pages 2021–2030, 2017. 1, 2, 3, 4, 6, 7

[34] Z. Zhang and V. Saligrama. Zero-shot learning via semantic similarity embedding. In *Proceedings of the IEEE international conference on computer vision*, pages 4166–4174, 2015. 1, 2, 3, 6, 7

[35] Z. Zhang and V. Saligrama. Zero-shot learning via joint latent similarity embedding. In *Proceedings of the IEEE Conference on Computer Vision and Pattern Recognition*, pages 6034–6042, 2016. 2, 3